26. Fe–Ti OXIDE MINERALOGY OF DSDP LEG 55 BASALTS

Masaru Kono, Geophysical Institute, University of Tokyo, Bunkyo-ku, Tokyo 113, Japan
David Clague, Middlebury College, Middlebury, Vermont
and
Edwin E. Larson, Department of Geological Sciences, University of Colorado, Boulder, Colorado

INTRODUCTION

Magnetic properties of volcanic rocks are controlled mainly by the physical and chemical state of their constituent ferromagnetic minerals. The most important parameters determining magnetic properties are concentration, composition, grain size, and oxidation state. In sea floor basalts, the main ferromagnetic minerals are titanomagnetites which are either unoxidized or, more commonly, have undergone various degrees of post-eruptive low-temperature oxidation to become cation-deficient titanomagnetites, or titanomaghemites. The effects of this low-temperature alteration are seen in the increase of Curie temperature and decrease of saturation magnetization and lattice parameter of ferromagnetic minerals (Readman and O'Reilly, 1972). It is now believed that titanomaghemitization of newly formed mid-ocean ridge crust proceeds with a time constant of about 1 m.y., accompanying drastic decrease of the intensity of the natural remanent magnetization (NRM) (Johnson and Atwater, 1977).

Titanomaghemites also occur in subaerial volcanic rocks (e.g., Akimoto and Kushiro, 1960) but such occurrence is not universal as in sea floor basalts, and is usually related to some form of hydrothermal alteration (Ade-Hall et al., 1971). Most subaerial basalts show varying degrees of high-temperature oxidation of titanomagnetites, which took place at temperatures higher than 600°C while the basalts cooled from the initial molten state (Buddington and Lindsley, 1964; Ozima and Larson, 1970).

Until now, the distinction between the ferromagnetic minerals in sea floor basalts and those in seamount basalts has not been adequately recognized. Lowrie (1977) pointed out a systematic difference in the intensity of NRM of DSDP and dredged samples, where dredged samples were obtained primarily near active oceanic ridges or seamounts and DSDP samples correspond to more or less ordinary sea floor. In detailed rock magnetic studies of dredged submarine rocks, Ozima et al. (1974) concluded that "regardless of the origin of submarine basalts whether they are from seamount or sea floor, the ferromagnetic mineral in young submarine basalts are homogeneous Ti-rich titanomagnetite, whereas titanomaghemite is the major ferromagnetic mineral in older submarine basalts." Marshall (1978) also found that the ferromagnetic minerals in Hole 192A basalt from Meiji Seamount are highly cation-deficient titanomagnetites quite similar to those found in other DSDP basalts drilled from the sea floor. Such a lack of distinction may be a result of insufficient sampling of seamount basalts; even on Meiji Seamount, only 13 meters of basaltic layer was penetrated.

Leg 55 of the Deep Sea Drilling Project (DSDP) offered a unique opportunity for studying seamount basalts. With penetrations into basaltic basement of 58.7 meters at Ōjin (Hole 430A), 31.9 meters at Nintoku (Hole 432A), and 10.5, 23 and 387.5 meters at Suiko (Holes 433A, 433B, 433C), it is now possible to study the magnetic properties of seamount basalts in detail. It is the purpose of this paper to investigate the physical and chemical states of ferromagnetic minerals in these basalts and to compare them with those in sea floor basalts. Using the results of rock magnetic studies (Kono, this volume), we hope to characterize the ferromagnetic minerals in Emperor Seamount basalts and to make a comparison of magnetic mineralogy of sea floor and seamount basalts.

OPTICAL MICROSCOPY

Polished sections of about a hundred samples were studied under oil immersion using a Reitz microscope with reflection light attachment. A magnification of 1000 was used throughout the study. The purpose of this observation was to define optically the oxidation state of the samples. The oxidation type of samples was already defined by Kono (this volume) from the shape of thermomagnetic curves, but the oxidation stage was independently defined from the microscopic observations.

The high-temperature oxidation stages used in the present study are developed from the scheme of Larson et al. (1969). Basically, low, moderate, and high oxidation stages were distinguished by the presence or absence and abundance of ilmenite lamellae in titanomagnetite host and pseudobrookite. Other phenomena, such as granulation (Ade-Hall et al., 1971), meta-ilmenites (oxidation product of ilmenite lamellae or ilmenite crystals, probably mixtures of pseudobrookite or rutile and hematite), and reddening and replacement of silicates by secondary iron oxides, were used as supporting evidence. Typical implications for each oxidation stage are as follows:

- N: No oxidation. Only homogeneous grains present. Indication of oxidation (ilmenite lamellae, etc.) absent.
- L: Low oxidation. Ilmenite lamellae not common. Silicates not affected.

M: Moderate oxidation. Abundant ilmenite lamellae present. Some silicates may show reddening and/or replacement. Pseudobrookite not common.

H: High oxidation. Most of the original titanomagnetites and ilmenites replaced by pseudobrookite, hematite, and meta-ilmenite. Reddening and replacement of silicates common.

When some samples showed intermediate stages or when different grains in a sample showed different stages, the samples were designated as L-M, etc. Since such determination cannot be purely objective, we did not try to express the oxidation stages by the numbering system of Wilson and Haggarty (1966) and Ade-Hall et al. (1968); but our stages N, L, M, H may correspond to their Classes 1, 1-2, 3, 4-6, respectively.

The oxidation stages defined in the foregoing do not take the secondary alteration into account. Some of the samples also contain titanomaghemites and show irreversible thermomagnetic curves (oxidation type LT, see Kono, this volume). In most of these samples, titanomaghemitization of minerals was ascertained by microscopic observation of shrinkage cracks and color change from brownish gray to bluish gray near grain boundaries and cracks (e.g., Johnson and Hall, 1978).

Results of microscopic observations are summarized in Tables 1, 2, and 3. In these tables, a close correlation can be seen between the oxidation type LT (irreversible thermomagnetic curve indicating titanomaghemite) and the optically observed titanomaghemites. Hence, it can be concluded that thermomagnetic analysis under moderately high vacuum ($\lesssim 10^{-4}$ Torr) is a good means for detecting titanomaghemites. If the ferromagnetic mineral is really one phase, measurements of the Curie point and the lattice parameter uniquely determine the composition of titanomaghemite (Readman and O'Reilly, 1972; T. Nishitani, in preparation).

Ferromagnetic minerals in Ōjin (Table 1) and Nintoku (Table 2) basalts show quite different oxidation conditions. Almost all the Ōjin samples show moderate to high oxidation, high Curie temperature, reversible thermomagnetic curve, and absence of secondary oxidation. On the other hand, many of the Nintoku samples have low to moderate Curie temperatures, irreversible thermomagnetic curves, and titanomaghemites. The original (high-temperature) oxidation was low to moderate in such samples. As they are alkalic basalts or hawaiites of similar ages drilled from similar depths of 1400 to 1600 meters, the basalts of the two seamounts may have experienced similar conditions at the time of eruption and afterwards. The difference in high-temperature oxidation states may have been caused by some local conditions, e.g., presence or absence of joints and cracks, availability of ground water, etc., at the time of initial emplacement. But at this stage, we cannot point out a plausible mechanism which caused such difference in oxidation environment.

In Suiko basalts, the degree of high-temperature oxidation is generally high, and most of the samples are free from the effects of low-temperature oxidation. Some of the minerals in lower oxidation stages show evidence of titanomaghemitization (Table 3). However, the occurrence of titanomaghemites seems unrelated to either the rock type (tholeiite or alkalic basalt) or the depth from the sea floor. Some of the lava flows contain both HT- and LT-type samples. The only distinction between these two types seems to be in the high-temperature oxidation stage. Figure 1 shows the histograms of Curie temperature and oxidation stages and a correction diagram between these two properties for all the Leg 55 samples. Apparently, the samples with titanomaghemites have undergone only low-temperature or low- to moderately high temperature oxidation. It is plausible that once the ferromagnetic minerals are highly oxidized at high temperatures, oxidation cannot proceed later at low temperatures even in a very oxidizing environment. High Curie temperature ($\gtrsim 500°C$) by itself does not mean a high degree of oxidation; when

TABLE 1
Reflection Microscopy of Fe–Ti Oxides, Hole 430A

Sample (Interval in cm)	Flow Unit	T_c	Type	Oxidation Stage	Ilmenite Lamellae	Pseudo-brookite	Titano-maghemite	Remarks
5-2, 30–32	1 (A)	520	HT	M-H	+++			
5-3, 107–109	1 (A)	503	HT	L				Homogeneous grains.
5-5, 44–46	2 (A)	575	HT	H	++	++		Ilmenite lamellae broken down to hematite and pseudobrookite. Olivines altered and contain patches of red hematite.
5-5, 103–105	2 (A)	583	HT	M-H	+++			
6-1, 67–69	2 (A)	575	HT	M-H	+++	+		Some silicate replaced by iron oxides.
6-1, 88–90	2 (A)	576	HT	M-H	+++			Some silicates replaced by iron oxides.
6-2, 54–56	3 (A)	582	HT	M-H	++			Titanomagnetite granulation. Patches of hematite.
6-2, 122–124	3 (A)	576	HT	M	+++			
6-4, 15–17	4 (A)	577	HT	M-H	+++			Replacement of silicates common.

Notes: Flow Unit column indicates flow unit number and type of rock: A, alkalic basalts, T, tholeiites. T_c = Curie temperature in °C. Type = type of thermomagnetic curve: NO, no oxidation, HT, high-temperature oxidation, LT, low-temperature oxidation. Oxidation Stage = degree of high-temperature oxidation of titanomagnetite: N, L, M, H = no, low, moderate, high oxidation. Ilmenite lamellae: presence of ilmenite lamellae in (111) planes of (titano-) magnetite host crystal. Pseudobrookite: presence of pseudobrookite as oxidation product of Ti-rich phase. Titanomaghemite: presence of low-temperature oxidation product. +++ abundant, ++ common, + present.

TABLE 2
Reflection Microscopy of Fe-Ti Oxides, Hole 432A

Sample (Interval in cm)	Flow Unit	T_c	Type	Oxidation Stage	Ilmenite Lamellae	Pseudo-brookite	Titano-maghemite	Remarks
2-1, 74–76	1 (A)	373	LT	L-M	+		+	Early stage of maghemitization indicated by bluish-gray tint and shrinkage cracks.
2-1, 107–109	1 (A)	364	LT	L-M	+		+	Low-grade maghemitization.
2-2, 23–25	2 (A)	575	HT	H	++	+++		Silicate replacement abundant. Ilmenite lamellae replaced by pseudobrookite and hematite.
2-2, 72–74	2 (A)	572	HT	M	+++	+		Reddening of silicate common.
2-3, 12–14	2 (A)	457	LT	L-M	++		+	Titanomagnetite shows blue-gray color. Shrinkage cracks present.
2-3, 21–23	2 (A)			L-M	++		++	Moderate maghemitization.
3-2, 67–69	3 (A)	187	NO	N				Homogeneous equant titanomagnetite crystals of 20 μm or less. Brown color.
4-1, 64–66	3 (A)	550	HT	M-H	+++	+		Abundant replacement of silicates.
4-1, 120–122	3 (A)	391	LT	L-M	++		++	Wide ilmenite lamellae. Some big grains 20–100 μm. Maghemitization shown by bluish-gray color and shrinkage cracks.
4-2, 80–82	3 (A)	577	HT	M	+++		trace	
5-2, 69–71	3 (A)	299	LT	L-M	+		+	Pyrite is present, filling cracks in silicates and oxides.

Note: See Table 1 for explanation.

the high-temperature oxidation is incomplete and there exist multiple ferromagnetic phases with a distribution of Curie temperatures, it is usually not possible to observe any but the highest Curie temperatures.

SCANNING ELECTRON MICROSCOPY

Some of the samples used in optical observations were repolished, etched 3 minutes in 6N hydrochloric acid, coated with evaporated gold, and observed using a scanning electron microscope (SEM). Since the number of samples observed by SEM is small, we do not claim that the following observations are characteristic of titanomagnetites in seamount basalts. However, the SEM observations illustrate several interesting features of the ferromagnetic minerals that could not be observed by any other means. The SEM used was a Cambridge Scientific Instruments model S4, equipped with a Kevex 5500 X-ray Energy Spectrometer, in the Department of Molecular Biology, University of Colorado, Boulder. Observations were carried out with an accelerating voltage of 20 kV and magnifications between 500 and 15,000. Some of the photographs are reproduced in Figures 2 through 4.

Figure 2a shows a titanomagnetite grain in Sample 432A-2-1, 74–76 cm at low magnification. The grain is homogeneous except for some irregular patches (dark gray) near some of the cracks and at the top right. The dark portion apparently corresponds to titanomaghemite. Since the low-temperature oxidation is not severe, the grain still keeps sharp boundaries, and shrinkage cracks are not common. Figure 2b shows a different grain from the same sample. Again the mild low-temperature oxidation resulted in dark, irregular patches near cracks. More irregular cracks appear in the figure, but it may be simply because the magnification was larger (5000 times) or it may represent the effect of volume change caused by oxidation. A notable feature of Figure 2b is the presence of minute ilmenite lamellae running parallel in two directions. These lamellae could not be observed by optical microscope, because of their small size. The SEM observations of this sample are consistent with the results of thermomagnetic and microscopic analyses (Table 2); high-temperature oxidation is mostly of low degree and there is indication of incipient titanomaghemitization.

Figure 3 shows a grain in Sample 432A-2-2, 72–74 cm at two magnifications. This sample is typical of the moderate (M) stage of high-temperature oxidation. The ilmenite lamellae are quite well developed. The thicker ones appear at spacings of about 2 μm; thinner ones are much more abundant, and their intervals are 0.5 μm or less. Undoubtedly, the subdivision by fine lamellae reduces the effective grain size and causes high magnetic stability similar to single domain grains (Strangway et al., 1968). The coercive force (H_c) and saturation remanence/magnetization ratio (J_r/J_s) of this sample are 288 Oe and 0.206 (Kono, this volume), in good agreement with the above conclusion.

Figure 4 shows Sample 430A-5-5, 44–46 cm, which is a highly oxidized sample, according to microscopic observation (Table 1). Figure 4a shows that in this grain, thick lamellae of 2 to 5 μm are well developed mostly in two directions. The matrix (lighter) part appeared homogeneous, but when we went up to a magnification of 6100 (Figures 4b, 4c), we observed a large number of tiny lamellae in the matrix part. As in Sample 432A-2-2, 72–74 cm (Figure 3), the tiny lamellae divide the titanomagnetite matrix into cells of 0.5 μm or less. Some of the thick lamellae contain dark patches (Figure 4b); perhaps they correspond to pseudobrookite, the oxidation product of ilmenite. This stage of oxidation is consistent with the microscopic observation, where some pseudobrookite is actually observed (Table 1).

The tiny lamellae in Figures 4b and 4c are aligned in two directions, neither of which is parallel to the directions of larger lamellae. As the ilmenite lamellae exsolve in (111) planes of spinel structure, there are usually three directions in which lamellae appear when a titano-

TABLE 3
Reflection Microscopy of Fe–Ti Oxides, Site 433

Sample (Interval in cm)	Flow Unit	T_c	Type	Oxidation Stage	Ilmenite Lamellae	Pseudo-brookite	Titano-maghemite	Remarks
Hole 433A								
20-2, 2–4	1 (A)	581	HT	M	+++			Some ilmenite altered to metailmenite. Mostly well-formed crystals of $\lesssim$ 30 μm. Some grains as large as 100 μm.
20-2, 14–16	1 (A)	580	HT	M	+++			Similar to above. Some pyrites present.
20-2, 24–26	1 (A)	580	HT	M	+++			Some silicates reddened.
Hole 433C								
10-3, 92–94	4 (T)	569	HT	H	+++	+++		Mostly skeletal crystals, extremely oxidized. Ilmenite lamellae and some silicates replaced.
10-3, 145–147	4 (T)	569	HT	M-H	+++	++		Variable oxidation stages in the sample. Grains near vesicles highly oxidized to pseudobrookite.
10-4, 69–71	4 (T)	572	HT	H	+++	+++		Similar to above. Very tiny grain present.
10-6, 38–40	5 (T)	574	HT	H	++	+++		Similar to above. Many silicates replaced.
11-1, 139–141	6 (T)	573	HT	H	++	+++		
11-3, 84–86	7 (T)	579	HT	M	+++			Granulation, metailmenites, reddening of silicates present.
11-3, 112–114	7 (T)	582	HT	L-M	+			Fine-scale granulation.
11-5, 36–38	8 (T)	539	HT	L+H	+	+++		Variable oxidation. Some grains homogeneous, others completely altered to pseudobrookite.
12-1, 109–111	9 (T)	554	HT	H	++	+++		Silicate reddened and replaced.
12-3, 5–7	9 (T)	264	LT	L-M	++		++	Shrinkage cracks.
13-2, 103–105	10 (T)	543	HT	M-H	++			Granulation and reddening common.
14-2, 37–39	11A(T)	574	HT	H				All microcrystals or skeletal crystals. Hematite very common, replaces original magnetite.
15-1, 17–19	11B(T)	376	LT	L-M	+		+	Many big crystals (<100 μm) and tiny skeletal grains (~1 μm). Few shrinkage cracks.
15-4, 48–50	12 (T)	551	HT	M-H		++		Very fine grained. Two states of oxidation. Near vesicles very high, others moderate.
15-4, 84–86	12 (T)	539	HT	M-H		++		Similar to above. Very fine grained quenched minerals.
15-5, 72–74	13 (T)	583	HT	M-H	+++	++		Hematite replaces magnetite. Silicates become very red.
16-1, 80–82	13 (T)	246	LT	L	+		+	Almost every titanomagnetite has ilmenite crystal attached to it. Either crystallized simultaneously or ilmenite separated by diffusion.
19-2, 9–11	14 (T)	576	HT	M-H	+++			Silicates very red.
19-2, 40–42	14 (T)	577	HT	H	+++	+++		Ilmenite lamellae altered to metailmenite. Some granulation present. Very red silicates.
19-2, 64–66	14 (T)	546	HT	H	+++	++		Similar to above. Lots of skeletal grains present.
19-3, 74–76	15A(T)	574	HT	L			+	Titanomagnetite grains have elongated shape, with no lamellae. Partly replaced by titanomaghemite.
20-1, 103–105	15B(T)	397	LT	L	+			Fine grains. Titanomaghemite not detected.
20-2, 20–22	15B(T)	334	LT	L-M	++			Some grains contain abundant ilmenite lamellae, others do not. Some pyrites present.
20-2, 35–37	15B(T)	367	LT	L	+		+	Some grains show granulation.
21-2, 128–130	16 (T)	520	HT	L+H	+	++		Variable oxidation, but mostly homogeneous grains with few lamellae. Some grains near vesicles show extremely high oxidation with pseudobrookite.
21-3, 7–9	17 (T)	532	HT	L-M	+			Smaller grains of euhedral shape are homogeneous. Larger grains (~50 μm) contain ilmenite lamellae.
21-4, 64–66	17 (T)	421	LT	L-M	+			Simple, well-formed crystals of the size 15~20 μm.
21-4, 101–103	17 (T)	375	LT	L-M	+		+	Granulation common in larger grains.
22-1, 104–106	18 (T)	537	HT	M-H	++	++		Hematite and reddening of silicates common.
25-2, 7–9	20 (T)	581	HT	M-H	+	++		Most magnetite grains are extremely fine-grained and appear in glass.
25-2, 27–29	20 (T)	570	HT	M-H	++	++		All opaque minerals granulated. Lamellae replaced by metailmenites.
25-2, 54–56	20 (T)	561	HT	L-M				Titanomagnetites very fine grained because of quenching. Silicates are not reddened.
25-5, 103–105	21 (T)	576	HT	M	+++			Little reddening of silicates.
26-5, 94–96	22 (T)	572	HT	L	+		+	Largest grains measure about 100 μm. Fine-scale granulation.

TABLE 3 – *Continued*

Sample (Interval in cm)	Flow Unit	T_c	Type	Oxidation Stage	Ilmenite Lamellae	Pseudo-brookite	Titano-maghemite	Remarks
Hole 433C								
26-6, 49–51	23 (T)	553	HT	M	+			Tiny grains exist in glass.
26-6, 129–131	23 (T)	535	HT	M	+			Ilmenites are large, bar-line crystals, but titanomagnetites are very small.
27-5, 41–43	24 (T)	541	HT	M				Quenched tiny crystals of titanomagnetite.
28-4, 121–123	26A (T)	580	HT	M-H				Titanomagnetites are fine grained. Very red silicates. Granulation common.
29-2, 115–117	26B (T)	492	LT	M-H				Very fine grained titanomagnetites in the glass. Very red silicates.
31-4, 83–85	28A (T)	562	HT	M-H				Same as above.
32-1, 38–40	28B (T)	558	HT	M-H		++		Same as above.
32-1, 112–114	28B (T)	582	HT	M-H				Same as above. Pyrites common.
35-1, 112–114	35 (T)	546	HT	M-H	++	++		Some granulation present. Grains are bigger.
35-6, 48–50	35 (T)	557	HT	L+H	++	+++		Variable oxidation states coexist: some grains are homogeneous with no lamellae, others contain pseudobrookite.
35-6, 121–123	36 (T)	573	HT	H	++	+++		All the titanomagnetites oxidized to hematite and pseudobrookite. Most silicates reddened and replaced.
35-7, 116–118	36 (T)	583	HT	M-H	++	++		Mostly small grains in glass, but also some larger grains of ~20 μm.
36-1, 45–47	36 (T)	576	HT	M	++			Skeletal grains. Silicates are reddened.
36-1, 105–107	37 (T)	577	HT	M	++			Similar to above.
36-3, 60–62	38 (T)	577	HT	M-H	++	++		Some large skeletal grains exist, but mostly small grains (2~3 μm). Silicates are reddened.
36-4, 56–58	39 (T)	528	HT	L-M				Fresh titanomagnetites of various size.
37-3, 74–76	44 (T)	534	HT	M	+			Very fine titanomagnetite grains abundant.
38-1, 57–59	45 (T)	577	HT	L-M				No lamellae but small-scale granulation present.
38-5, 119–121	47 (T)	364	LT	L			+	Small-scale granulation. Some grains have cracks.
39-5, 96–98	48 (T)	581	HT	L-M				Some granulation. Silicates slightly reddened.
39-6, 78–80	48 (T)	573	HT	L-M				Same as above.
41-1, 51–53	51B (T)	573	HT	M-H	+++	++		Silicates reddened.
42-1, 68–70	52 (T)			M-H	+++	++		Same as above.
42-2, 136–138	53 (T)	573	HT	M-H	+++	++		Same as above.
42-5, 134–136	54 (T)	425	LT	M	++	+	+	Small and large (up to 200 μm) grains coexist. A few maghemite cracks.
43-1, 33–35	54 (T)	578	HT	H	+++	+++		Silicates reddened.
44-1, 41–43	56 (T)	578	HT	M-H				Abundant small crystals highly oxidized and appear reddened.
44-4, 108–110	58 (T)	553	HT	M				Abundant fine titanomagnetite grains. Some granulation and reddening of silicates.
45-2, 45–47	59 (T)	553	HT	M				Similar to above.
45-5, 51–53	60 (T)	371	LT	L-M	+		+++	Larger grains are not much HT oxidized.
45-6, 43–45	60 (T)	431	LT	L-M	++		++	Larger grains with ilmenite lamellae.
46-3, 54–56	60 (T)	579	HT	H	++	+++		Pseudobrookite, metailmenite, reddening and replacement of silicate very abundant.
47-1, 26–28	63 (T)	579	HT	M	++			Large and small grains of titanomagnetite. Some granulation.
47-5, 25–27	64 (A)	472	LT	M				Well-formed, equant crystals with some granulation.
48-3, 30–32	64 (A)	575	HT	M-H	+++	++		Reddened silicates abundant.
49-1, 142–144	66 (T)	577	HT	M-H	+++	++		Same as above.
49-2, 50–52	66 (T)	575	HT	M-H	++	++		Similar to above.

Note: See Table 1 for explanation.

magnetite grain is cut at an arbitrary surface. The directions defined by tiny lamellae in Figure 4b are all different from the directions of larger lamellae. Such difference is possible if the materials of the large and small lamellae are different. In fact, in some rocks, ulvospinel lamellae appear in (100) planes of magnetite because of solvus reaction. In the present sample, ulvospinel cannot be the material, since the oxidation state is high, but some other cubic material may really make up the tiny lamellae. A series of X-ray energy-dispersive spectra were taken by Kevex spectrometer. The portions where spectra shown in Figure 5 were obtained are marked in Figures 4a and 4b. Figure 5a shows the spectrum inside a thick ilmenite lamella in Figure 4b. Apart from peaks of gold at about 2 and 10 keV (representing the sample surface coating), only the peaks of Ti and Fe rise above the noise level. Because the spectrometer is not calibrated for quantitative analysis, it is not possible to deter-

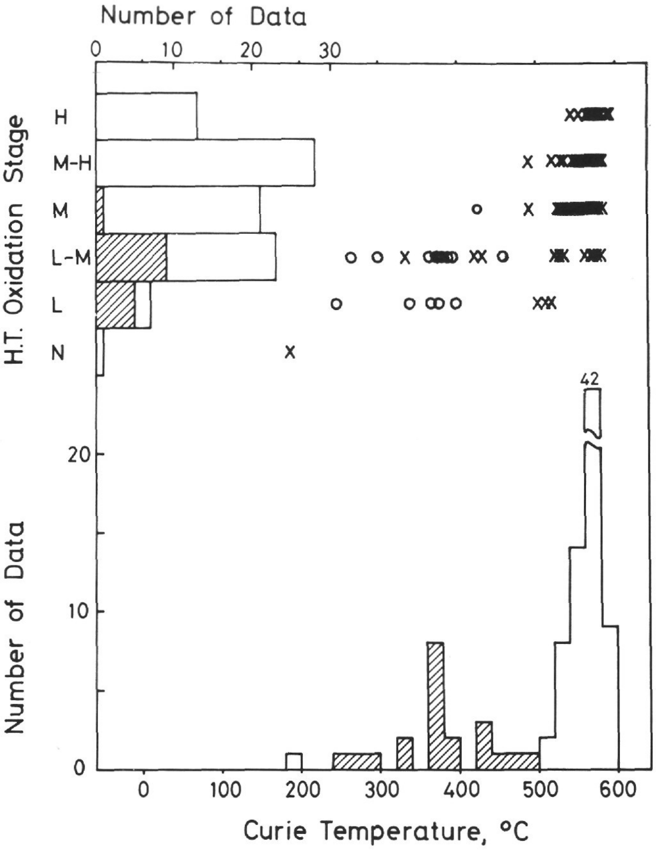

Figure 1. *Histograms of Curie points (bottom) and high-temperature oxidation stages (upper left) and the correlation between these two properties (upper right). Samples containing low-temperature-oxidized phase are indicated by hachures and circles.*

mine the exact ratio of Fe atoms to Ti atoms. It is reasonable to assume, however, that the ratio is close to 1, corresponding to the composition of ilmenite. Figure 5b shows the spectrum from another portion of Figure 4b. Since it is not possible to determine the composition of tiny lamellae, a mixture of lamellae and groundmass was measured. Figure 5b shows that Ti is almost absent from this part, and that a considerable amount of Al is present in addition to Fe. Mg may also be present, but we cannot be sure, because of the high background noise level near 1 keV. Figure 5c is a spectrum taken from a much larger area of the same grain (Figure 4a), and can be taken to represent the overall composition of this grain. Here, the Fe and Ti peaks are dominant, but the presence of Al and Mg is also certain. From Figure 5b alone, we might have concluded that the tiny lamella is composed of either hercynite ($FeAl_2O_4$) or spinel ($MgAl_2O_4$), both of which have spinel structure. Since Mg apparently exists in this grain, however, it is more plausible that the tiny lamellae are of spinel composition. Lamella structure of spinel in titanomagnetite has not been reported, to our knowledge, but is plausible, since Katsura et al. (1976) report that spinel forms a perfect solid solution with titanomagnetite at high temperatures in the $TiFe_2O_4$-Fe_3O_4-$MgAl_2O_4$ ternary system, provided that the $MgAl_2O_4$ concentration is less than about 20 per cent. Mg and Al are also the most abundant "impurity" atoms in naturally occurring titanomagnetites (e.g., Creer and Ibbetson, 1970). Another important implication is that the matrix becomes very Ti-poor and tends toward almost pure magnetite (Fe_3O_4) as the oxidation proceeds and lamellar structure develops, as shown in Figure 5b.

In the SEM studies, it was not possible to distinguish hematite from unoxidized magnetite. We do not know if this is a general limitation of SEM. But supplementary optical-microscopic observations can alleviate this deficiency quite well. The magnification of 15,000 is not a limit of SEM capability, but at higher magnifications, the images are so blurred that a good view cannot be obtained. This is perhaps a result of the magnetic field caused by minerals, which deflects the electron beams out of focus. A range of 1000 × to 10,000 × may be the optimum range for SEM observation of titanomagnetites.

X-RAY MICROPROBE ANALYSES

Results of microprobe analyses are summarized in Tables 4 through 6. These tables list weight percentages of TiO_2, Al_2O_3, Cr_2O_3, FeO, MgO, MnO, and the totals, as well as composition parameters x or y for titanomagnetite, $xFe_2TiO_4 \cdot (1-x)Fe_3O_4$, or hemoilmenite, $yFeTiO_3 \cdot (1-y)Fe_2O_3$. The composition parameters were calculated using the following scheme. The x values were calculated directly from Ti/Fe ratios. Al, Cr, Mg, and Mn were assumed as impurities. Some grains contain a considerable amount of Cr; but in all cases there is enough Mg to form magnesiochromite ($MgCr_2O_4$), so that our assumption is perhaps valid. In the derivation of y, TiO_2 was assumed to be distributed among the ternary system geikielite ($MgTiO_3$)-pyrophanite ($MnTiO_3$)-hemoilmenite. This assumption was necessary because in many crystals Ti/Fe ratio exceeds one, indicating y values larger than 1. As geikielite and pyrophanite have the same crystal structure ($R\bar{3}$) as ilmenite, and as they are known to form solid solution with ilmenite, this assumption seems well founded. Al and Cr are again neglected in the calculation as impurities. Geikielite and pyrophanite component is about 10 mole per cent or less for most grains, but a few contain more than 20 mole per cent of these minerals.

Many of the data show low totals of 90 to about 95 per cent. Part of this mass deficiency is caused by taking total iron as FeO. If we calculate the proper amount of Fe_2O_3 for each grain, part of the discrepancy can be accounted for. Since the electron beam of the microanalyzer is a few micrometers across, we are looking at some average composition of a grain. As the results of optical and electron microscopic observations show, most of our samples are oxidized to some extent. This means that the "titanomagnetite" phase may be either a mixture of ilmenite and magnetite or even a mixture of pseudobrookite and hematite. A similar situation exists with regard to the "hemoilmenite" phase. In such cases, we have more Fe_2O_3 at the expense of FeO. But all the mass deficiency cannot be attributed to $Fe^{2+} \rightarrow Fe^{3+}$ changes, for two reasons: first, the deficiency remains in

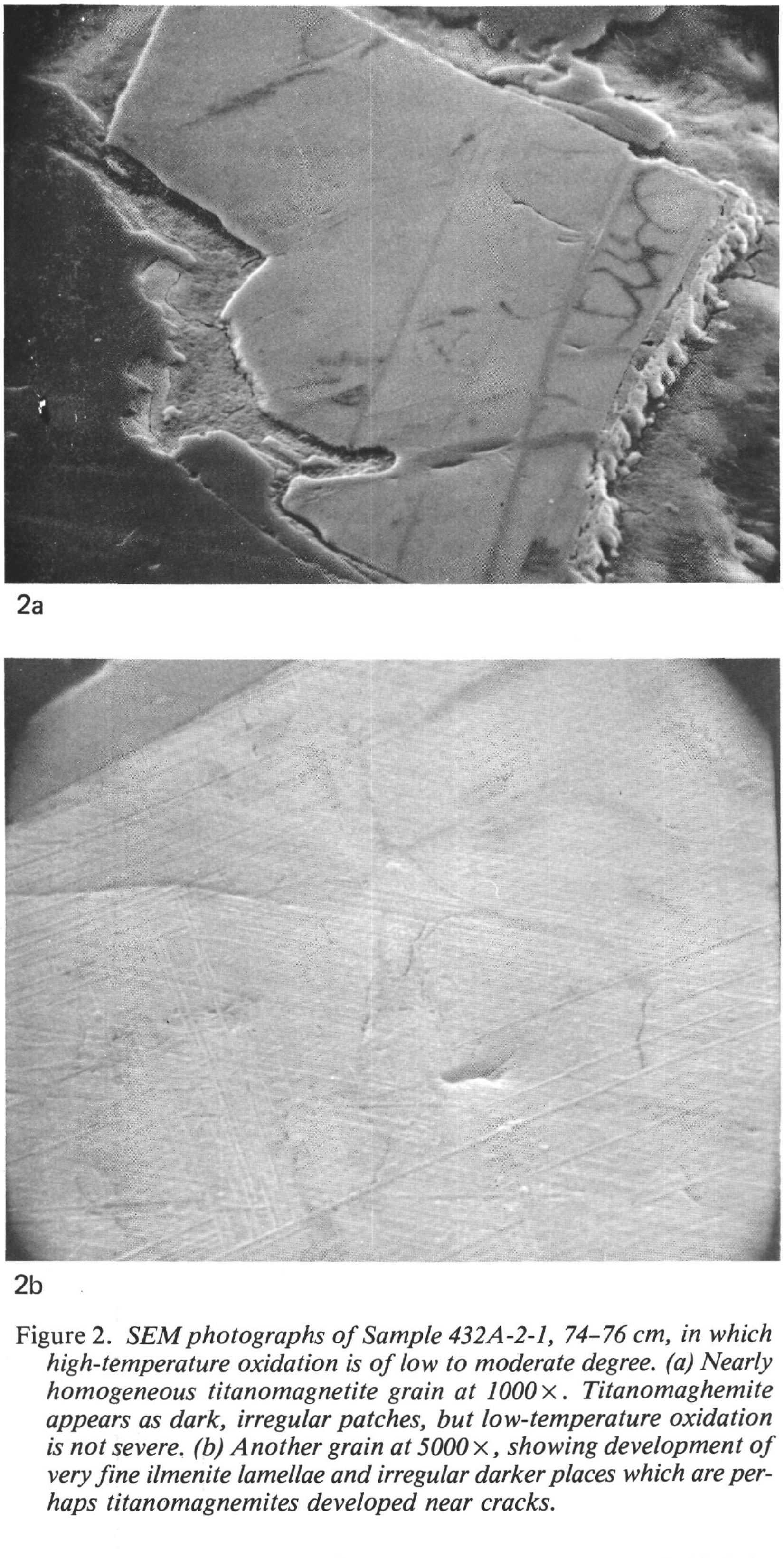

Figure 2. *SEM photographs of Sample 432A-2-1, 74–76 cm, in which high-temperature oxidation is of low to moderate degree. (a) Nearly homogeneous titanomagnetite grain at 1000×. Titanomaghemite appears as dark, irregular patches, but low-temperature oxidation is not severe. (b) Another grain at 5000×, showing development of very fine ilmenite lamellae and irregular darker places which are perhaps titanomagnemites developed near cracks.*

some samples even after we take all the iron as Fe^{3+}; second, such a method of calculation would give a wide range of oxidation parameter z for grains closely located in the same sample — for instance, in Sample 432A-5-2, 57–66 cm, z ranges from 0.15 to 0.73, which is quite unrealistic. Therefore, the deficiency may show the effects of oxidation, as well as other impurity atoms (such as vanadium) not measured in our experiments.

Figure 6 shows the histograms of x and y for the present samples. The value of x or y of each grain is counted

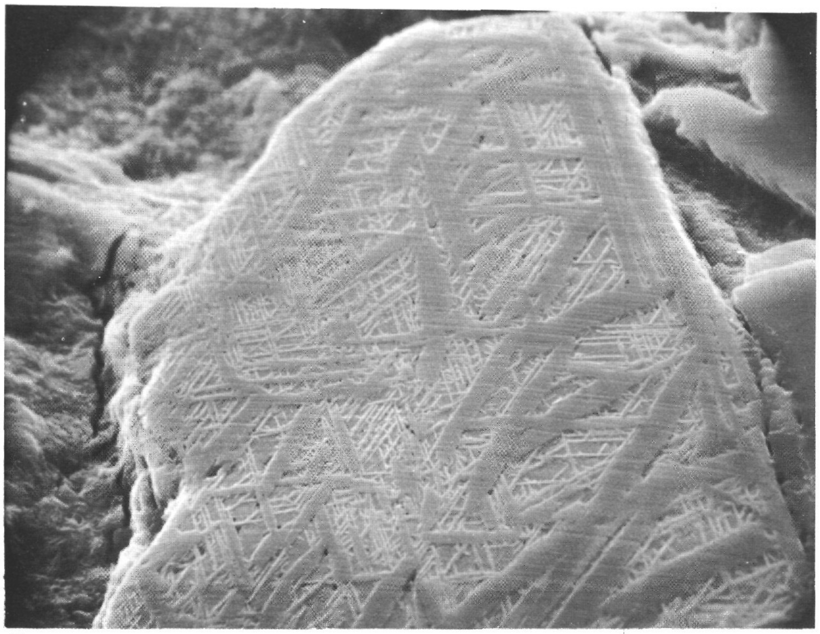

3a

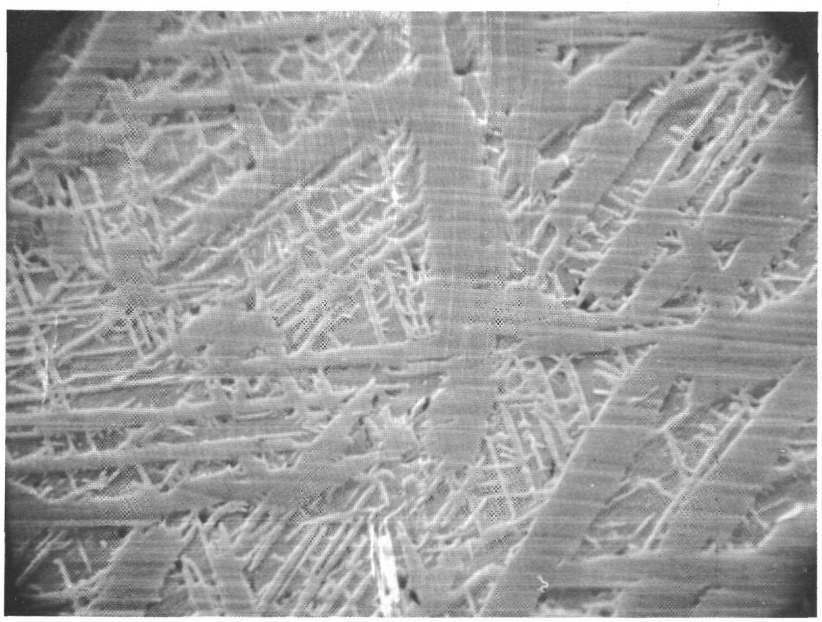

3b

Figure 3. *SEM photographs of Sample 432A-2-2, 72–74 cm, which is a typical example of moderate stage of high-temperature oxidation. (a) A titanomagnetite grain at a magnification of 2360×. (b) The same grain at 5800×. Note the development of very fine ilmenite lamellae (rod shaped).*

as a datum in this figure, but the distributions are not much different when sample-average x and y (Table 7) are used. This figure shows that most of the hemoilmenite grains have a composition in a narrow range, $0.9 < y < 1.0$, whereas the titanomagnetite grains show a wide variety in their composition centered around $x \approx 0.7$. In ocean floor basalts, x of almost all the titanomagnetite (titanomaghemite) grains fall between 0.5 and 0.7, with a mean value of about 0.65 (Johnson and Hall, 1978; Hamano et al., 1979). A wide range of x values may be a characteristic property of subaerial basalts. Petersen (1976) summarized 237 analyses of titanomagnetites in basalts excluding ocean floor basalts, and obtained a mean of $x = 0.61$. The x values in his analysis range between 0.1 and 0.9, while all the hemoilmenites have composition in the range $0.8 < y < 10$. The wide varia-

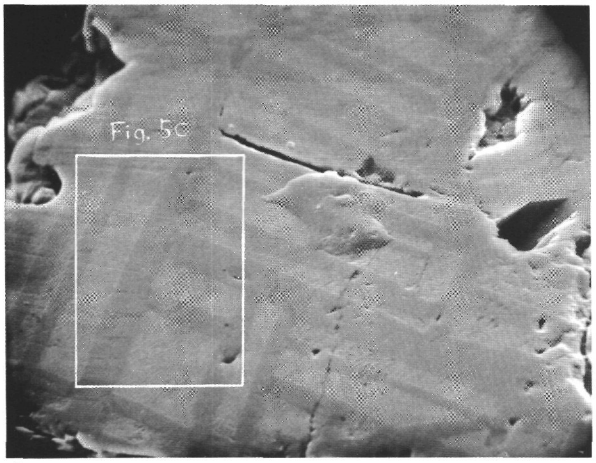

4a

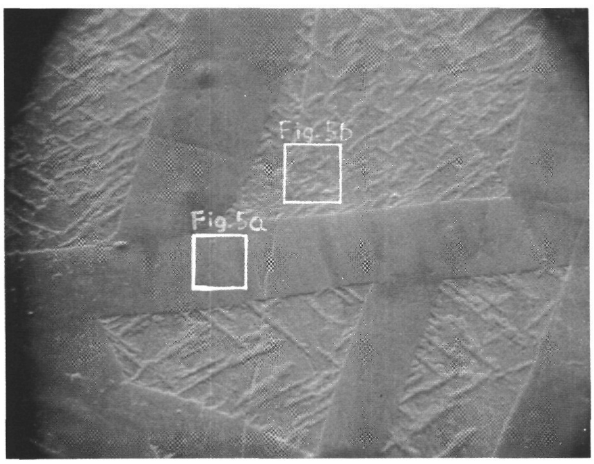

4b

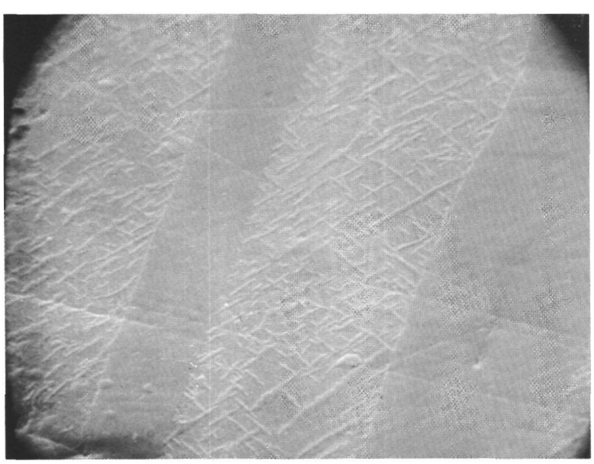

4c

Figure 4. *SEM photographs of Sample 430A-5-5, 44–46 cm, showing high stage of high-temperature oxidation. The areas of analyses of X-ray energy-dispersive spectra in Figure 5 are indicated by rectangles. (a) Titanomagnetite grain with ilmenite lamellae (darker bars) at a magnification of 1200×. (b), (c) Different parts of the same grain at 6100×. Note that the very tiny lamellae in the matrix are not parallel to the thicker ones, suggesting that they are of different crystal structure.*

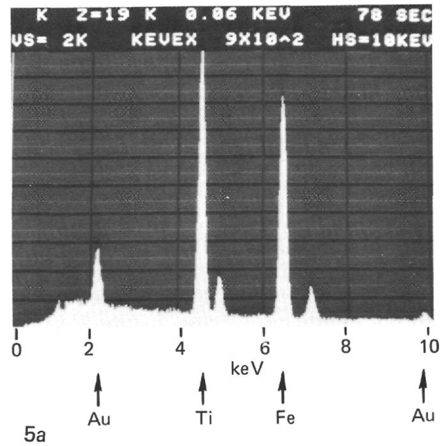

5a

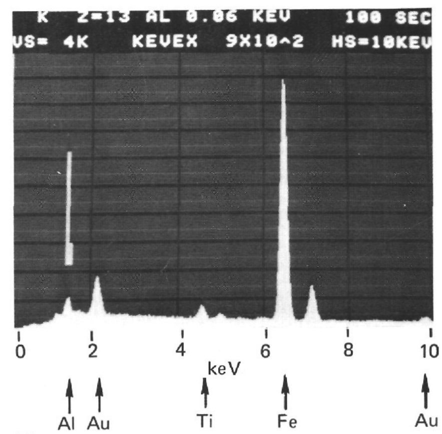

5b

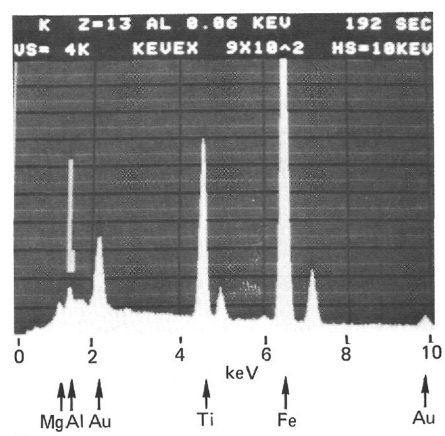

5c

Figure 5. *Energy-dispersive spectra of portions of titanomagnetites in Sample 430A-5-5, 44–46 cm. Relevant energy peaks are Fe, 6.4 keV (K_α), 7.1 keV (K_β); Ti, 4.5 keV (K_α), 4.9 keV (K_β); Al, 1.5 keV; Mg, 1.3 keV. The peaks near 2 keV and 10 keV are due to Au-coating of samples. (a) Inside an ilmenite lamella in Figure 4b, where Ti and Fe peaks dominate. (b) In matrix part in Figure 4b, where tiny lamellae exsolve. Note that Ti peak is very low and that Al is clearly present, while Mg peak is barely out of the background. The bars above the Al peak indicate expected K_α and K_β emission lines of Al. (c) Overall composition. This time the Mg peak is more clearly evident.*

TABLE 4
Microprobe Analysis of Fe–Ti Oxides, Site 430 Basalts

No.	TiO_2	Al_2O_3	Cr_2O_3	FeO	MgO	MnO	Total	Titano-magnetite:x	Hemo-ilmenite:y
				430A-4-2, 110–118 cm					
1	19.61	0.95	0.00	69.99	2.26	0.38	93.19	0.604	
2	19.63	0.64	0.00	69.76	2.38	0.43	92.84	0.606	
3	21.41	0.63	0.00	68.45	2.71	0.44	93.64	0.659	
4	30.70	0.40	0.00	59.84	1.88	0.24	93.06	0.947	
5	31.67	0.47	0.00	61.16	1.91	0.29	95.50	0.953	
6	40.31	0.45	0.00	49.90	3.08	0.68	94.42		0.753
7	41.98	0.31	0.00	49.58	3.90	0.65	96.42		0.756
8	49.09	0.21	0.00	46.14	2.73	0.68	98.85		0.911
9	52.01	0.21	0.00	37.07	3.34	0.41	93.04		1.043
				430A-5-1, 21–27 cm					
10	14.87	1.62	0.00	76.75	0.93	0.39	94.56	0.445	
11	37.82	0.24	0.00	53.93	1.36	0.23	93.58		0.735
12	43.50	0.16	0.00	50.41	1.88	0.35	96.30		0.825
13	44.64	0.34	0.00	48.28	2.50	0.45	96.21		0.844
14	44.44	0.26	0.00	48.13	2.46	0.44	95.73		0.844
15	49.18	0.30	0.00	44.62	3.13	0.49	97.72		0.922
16	49.71	0.26	0.00	41.88	3.04	0.50	95.39		0.962
17	50.25	0.16	0.00	44.55	2.89	0.48	98.33		0.941
18	50.85	0.18	0.00	40.73	3.55	0.56	95.87		0.976
19	51.71	0.17	0.00	42.32	3.18	0.60	97.98		0.975
20	55.27	0.23	0.00	38.23	2.37	0.44	96.54		1.082
				430A-5-2, 102–115 cm					
21	17.38	1.45	0.00	73.74	1.72	0.44	94.73	0.525	
22	16.38	1.05	0.00	75.23	1.04	0.46	94.16	0.491	
23	16.73	0.93	0.00	74.92	0.95	0.37	93.90	0.502	
24	18.41	1.09	0.03	72.75	1.25	0.42	93.95	0.556	
25	17.28	1.31	0.03	73.41	1.36	0.43	93.82	9.524	
26	46.97	0.18	0.00	45.13	2.44	0.46	95.18		0.907
27	47.33	0.14	0.00	45.77	2.30	0.50	96.04		0.907
28	46.45	0.17	0.00	46.36	2.01	0.49	95.48		0.897
29	47.27	0.16	0.00	46.41	2.15	0.48	96.47		0.903
				430A-6-1, 17–25 cm					
30	16.60	0.82	0.03	72.79	1.47	0.59	92.30	0.511	
31	22.71	0.64	0.01	70.64	0.74	0.42	95.16	0.673	
32	15.60	0.96	0.00	73.11	1.25	0.61	91.53	0.483	
33	19.84	0.81	0.00	71.12	0.95	0.34	93.06	0.602	
34	21.58	0.84	0.00	69.57	1.16	0.46	93.61	0.654	
35	49.29	0.19	0.00	47.20	1.84	0.50	99.02		0.924
36	48.91	0.19	0.00	45.73	3.08	0.52	98.43		0.907
37	50.05	0.18	0.00	45.06	2.84	0.57	98.70		0.933
38	49.31	0.14	0.00	46.28	2.93	0.57	99.23		0.909
				430A-6-3, 52–63 cm					
39	22.10	1.50	0.00	68.86	2.39	0.65	95.50	0.672	
40	23.48	0.77	0.00	66.82	2.20	0.59	93.86	0.720	
41	18.93	1.02	0.05	72.50	1.35	0.45	94.30	0.570	
42	21.14	1.36	0.04	70.36	2.20	0.55	95.65	0.638	
43	22.95	1.14	0.02	68.59	1.91	0.64	95.25	0.694	
44	51.25	0.14	0.27	42.45	1.68	0.29	96.08		1.004
45	51.27	0.16	0.50	43.48	2.24	0.50	98.15		0.978
46	54.43	0.11	0.00	40.75	2.12	0.39	97.80		1.047
47	50.58	0.19	0.50	44.63	2.11	0.63	98.64		0.959
48	46.67	0.12	0.43	46.95	1.14	0.58	95.89		0.912
				430A-6-4, 7–15 cm					
49	22.07	0.76	0.00	69.20	1.39	0.44	93.86	0.669	
50	17.05	0.98	0.00	73.65	1.08	0.41	93.17	0.517	
51	17.83	0.61	0.00	73.15	0.84	0.29	92.72	0.539	
52	20.63	1.05	0.00	69.58	1.42	0.33	93.01	0.631	
53	19.98	1.33	0.00	70.51	1.52	0.50	93.84	0.609	
54	47.60	0.40	0.00	43.95	2.69	0.71	95.35		0.918
55	52.68	0.23	0.00	41.25	1.67	0.32	96.15		1.033
				430A-6-4, 140–150 cm					
56	25.20	1.23	0.00	66.28	1.40	0.82	94.93	0.764	
57	22.65	0.79	0.00	68.82	0.88	0.63	93.77	0.685	
58	23.37	1.01	0.00	68.43	0.76	0.45	94.02	0.705	
59	19.74	1.35	0.03	72.98	0.80	0.50	95.40	0.587	
60	49.56	0.17	0.00	48.25	1.42	0.34	99.73		0.927
61	49.30	0.20	0.12	48.09	1.46	0.32	99.49		0.925

TABLE 5
Microprobe Analysis of Fe–Ti Oxides, Site 432 Basalts

No.	TiO_2	Al_2O_3	Cr_2O_3	FeO	MgO	MnO	Total	Titano-magnetite:x	Hemo-ilmenite:y
				432A-2-1, 86–92 cm					
1	27.57	1.49	0.01	64.96	0.38	0.60	95.01	0.829	
2	28.54	1.57	0.00	63.22	1.02	0.71	95.06	0.866	
3	28.44	0.81	0.00	61.96	1.29	0.68	93.18	0.876	
4	27.44	0.91	0.00	66.71	0.58	0.56	96.20	0.810	
5	27.94	0.62	0.00	66.00	0.61	0.72	95.89	0.827	
6	27.00	0.63	0.00	66.20	0.71	0.55	95.09	0.805	
7	30.54	1.32	0.20	60.17	1.06	0.69	93.98	0.940	
				432A-2-3, 37–43 cm					
8	33.39	1.82	0.00	57.38	1.11	1.02	94.72		0.640
9	32.23	1.41	0.00	57.92	1.20	1.09	93.85		0.615
10	27.73	1.84	0.00	61.61	1.13	0.61	92.92	0.864	
11	26.91	1.60	0.00	60.46	1.50	0.62	91.09	0.858	
12	26.61	1.72	0.62	62.87	0.82	0.77	93.41	0.827	
				432A-3-2, 120–126 cm					
13	22.57	1.55	0.08	68.66	2.97	0.68	96.51	0.684	
14	22.61	1.41	0.07	69.31	2.63	0.65	96.68	0.680	
15	21.75	1.63	0.02	67.76	2.71	0.74	94.61	0.672	
16	22.37	1.19	0.06	68.30	2.21	0.68	94.81	0.683	
17	22.43	1.57	0.02	68.33	2.58	0.69	95.62	0.684	
				432A-5-2, 57–66 cm					
18	27.52	1.33	0.25	65.91	2.35	0.58	97.94	0.819	
19	26.61	1.36	0.00	64.92	1.79	0.76	95.44	0.808	
20	27.41	1.43	0.09	65.88	2.33	0.60	97.74	0.817	
21	27.07	1.19	0.39	63.66	0.91	1.31	94.53	0.830	
22	27.04	1.36	0.20	65.91	1.96	0.58	97.05	0.808	
23	27.55	1.25	0.21	63.55	2.17	0.80	95.53	0.841	
24	27.22	1.16	0.27	66.00	1.86	0.59	97.10	0.812	

tion of x may be a result of diffusion of metallic ions (Fe, Ti) at high temperatures when high temperature oxidation is proceeding.

Sample-average compositions of titanomagnetites and hemoilmenites in Leg 55 basalts are shown in Table 7. Where four or more determinations of both x and y are available, the temperature and oxygen fugacity *(fO_2)* of equilibration were estimated by the method of Buddington and Lindsley (1964) and also given in this table. The temperatures and oxygen fugacities thus obtained range between 790 and 1200°C and $10^{-8.2}$ and $10^{-16.4}$ atm, respectively, but mostly lie between 960°C and 1100°C and between 10^{-10} and 10^{-12} atm. These data distribute close to the fayalite–magnetite–quartz (FMQ) buffer in the temperature versus oxygen fugacity diagram, in agreement with the data of Carmichael and Nicholls (1967). As discussed earlier, the composition of a mineral grain determined by microanalyzer is an average of an area a few micrometers across. In the present samples, however, chemical homogeneity cannot usually be expected for such an area in a grain, because the high-temperature oxidation caused the unmixing of titanomagnetite into Ti-rich and Ti-poor phases even at the sub-micrometer level. Therefore, these estimates should correspond to conditions at which separate titanomagnetite and hemoilmenite minerals were crystallized. Some of the samples show much lower temperature than the others (430A-6-3, 52–63 cm and 433C-42-1, 56–63 cm). They may correspond to the times when larger (~5 μm) ilmenite lamellae unmixed from the titanomagnetite host by high-temperature oxidation. It is quite certain that the Buddington–Lindsley method gives only the last equilibrium condition *at some size level.* High-temperature oxidation still proceeds at lower temperatures, but we cannot measure compositions of separate phases at this stage, because they are too small.

TABLE 6
Microprobe Analysis of Fe–Ti Oxides, Site 433 Basalts

No.	TiO_2	Al_2O_3	Cr_2O_3	FeO	MgO	MnO	Total	Titano-magnetite:x	Hemo-ilmenite:y
				433A-20-1, 30–36 cm					
1	23.39	0.91	0.00	66.47	1.45	0.68	92.90	0.721	
2	22.32	1.02	0.00	68.61	1.29	0.64	93.88	0.679	
3	21.66	1.04	0.00	69.67	1.20	0.69	94.26	0.655	
4	21.07	1.15	0.00	70.84	1.27	0.62	94.95	0.633	
5	19.86	0.54	0.00	72.59	0.50	0.52	94.01	0.592	
				433A-21-4, 129–138 cm					
6	25.67	1.06	0.14	67.31	1.27	0.45	95.90	0.766	
7	19.96	1.38	0.00	71.83	1.42	0.42	95.01	0.600	
8	19.41	1.56	0.00	70.42	1.56	0.48	93.43	0.596	
9	17.50	1.43	0.00	74.46	0.84	0.52	94.75	0.523	
10	14.88	1.71	0.00	75.21	1.32	0.41	93.53	0.453	
11	14.40	1.40	0.00	75.97	1.02	0.45	93.24	0.437	
12	54.36	0.18	0.00	41.33	1.92	0.51	98.30		1.042
13	47.08	0.39	0.00	47.64	2.31	0.68	98.10		0.881
				433B-5-2, 61–68 cm					
14	21.54	1.10	0.00	71.63	1.03	0.50	95.80	0.639	
15	25.81	0.94	0.00	67.81	1.31	0.63	96.50	0.765	
16	25.61	1.01	0.00	67.54	1.68	0.62	96.46	0.763	
17	21.21	1.46	0.00	69.87	1.25	0.52	94.31	0.643	
18	20.08	1.00	0.00	73.70	0.74	0.53	96.05	0.590	
19	50.43	0.13	0.00	46.97	1.64	0.59	99.76		0.942
20	49.18	0.19	0.00	47.43	1.30	0.64	98.74		0.930
				433B-5-3, 85–90 cm					
21	21.55	1.01	0.00	69.15	1.40	0.59	93.70	0.657	
22	21.11	1.60	0.00	66.53	1.66	0.41	91.31	0.666	
23	22.92	1.27	0.00	65.95	1.68	0.56	92.38	0.714	
24	23.43	1.25	0.00	66.01	1.75	0.56	93.00	0.726	
25	20.24	0.85	0.85	70.57	0.47	0.56	92.69	0.615	
				433C-4-1, 30–38 cm					
26	24.53	1.03	0.00	70.56	1.23	0.61	97.96	0.714	
27	23.06	1.32	0.00	69.60	1.54	0.57	96.09	0.689	
28	23.62	1.12	0.02	70.08	1.63	0.68	97.15	0.698	
29	22.77	1.24	0.00	70.72	1.10	0.54	96.37	0.674	
30	23.80	1.05	0.02	70.54	1.54	0.62	97.57	0.698	
31	48.75	0.16	0.00	47.12	1.70	0.60	98.33		0.921
32	48.24	0.18	0.00	46.49	1.80	0.59	97.30		0.920
33	48.49	0.17	0.00	46.80	1.75	0.59	97.80		0.920
34	20.22	3.21	7.17	63.77	2.57	0.67	97.61	0.666	
35	22.29	2.54	3.68	65.97	2.49	0.62	97.59	0.699	
36	19.51	3.75	7.82	64.01	3.05	0.63	98.77	0.645	
				433C-10-4, 11–17 cm					
37	24.95	0.75	0.00	62.65	2.06	0.25	90.66	0.791	
38	19.03	0.57	0.00	70.70	1.65	0.25	92.20	0.585	
39	17.59	0.51	0.00	72.17	1.78	0.26	92.31	0.539	
40	9.71	1.30	0.04	79.76	2.09	0.54	93.44	0.296	
41	24.11	1.67	1.96	60.88	5.14	0.58	94.34	0.788	
				433C-12-3, 57–65 cm					
42	23.69	2.70	0.00	65.61	0.99	0.33	93.32	0.735	
43	21.26	2.54	0.00	66.60	1.25	0.63	92.28	0.669	
44	20.91	2.30	0.00	69.38	0.88	0.45	93.92	0.640	
45	12.82	3.10	0.00	76.76	0.61	0.43	93.72	0.392	
46	4.44	1.75	0.06	79.59	0.92	0.27	87.03	0.143	
				433C-13-2, 55–66 cm					
47	25.80	0.93	0.00	68.77	0.75	0.68	96.93	0.757	
48	26.25	1.46	0.00	67.66	1.36	0.57	97.30	0.776	
49	26.86	1.44	0.00	66.16	1.43	0.77	96.66	0.802	
50	25.02	1.66	0.00	68.76	1.34	0.61	97.39	0.740	
51	26.71	1.38	0.00	66.89	1.44	0.71	97.13	0.793	
52	49.76	0.19	0.00	47.87	1.41	0.45	99.68		0.932
53	50.66	0.16	0.00	46.27	1.92	0.42	99.43		0.948
54	50.45	0.22	0.00	47.46	1.64	0.50	100.27		0.938
55	50.20	0.23	0.00	46.75	1.96	0.50	99.64		0.936
56	50.30	0.19	0.00	47.04	1.76	0.48	99.77		0.939
				433C-14-3, 8–15 cm					
57	27.66	1.92	0.00	61.82	0.79	0.40	92.59	0.861	
58	21.66	1.61	0.00	68.63	0.66	0.34	92.90	0.663	
59	26.12	1.80	0.00	64.59	0.56	0.36	93.43	0.800	
60	27.15	1.85	0.00	62.69	0.82	0.42	92.93	0.841	
61	28.48	1.54	0.00	61.99	1.10	0.41	93.52	0.877	
62	49.55	0.22	0.00	47.70	0.81	0.54	98.82		0.943
63	50.91	0.26	0.00	46.15	0.95	0.44	98.71		0.972
64	49.00	0.27	0.00	47.26	0.70	0.52	97.75		0.944
65	53.99	0.22	0.00	41.95	0.97	0.40	97.53		1.051
66	50.59	0.23	0.00	45.68	0.87	0.46	97.83		0.975
				433C-15-6, 16–31 cm					
67	26.14	2.03	0.00	65.33	1.46	0.46	95.42	0.794	
68	24.46	1.21	0.00	67.22	1.69	0.51	95.09	0.740	
69	21.20	2.26	0.00	70.36	1.46	0.39	95.67	0.640	
70	23.81	1.36	0.00	66.89	1.00	0.46	93.52	0.727	
71	25.95	1.97	0.00	63.27	1.14	0.36	92.69	0.808	
72	24.67	1.23	0.00	65.65	0.98	0.41	92.94	0.758	
73	49.54	0.30	0.00	44.38	1.93	0.48	96.63		0.956
74	52.41	0.21	0.00	42.61	1.00	0.48	96.71		1.026

TABLE 6 – *Continued*

No.	TiO_2	Al_2O_3	Cr_2O_3	FeO	MgO	MnO	Total	Titano-magnetite:x	Hemo-ilmenite:y
				433C-19-5, 57–65 cm					
75	21.98	0.99	0.00	68.09	0.53	0.30	91.89	0.675	
76	22.62	1.36	0.00	68.75	0.57	0.31	93.61	0.685	
77	23.88	1.68	0.00	65.09	0.69	0.47	91.81	0.744	
78	48.39	0.17	0.00	47.03	0.94	0.33	96.86		0.938
79	48.19	0.15	0.00	46.36	1.02	0.38	96.10		0.940
80	49.78	0.23	0.00	44.87	1.12	0.34	96.34		0.972
81	48.59	0.21	0.00	46.31	0.93	0.25	96.29		0.949
82	48.84	0.16	0.00	46.61	0.94	0.34	96.89		0.947
				433C-21-4, 7–13 cm					
83	14.89	1.13	0.00	70.40	1.85	0.35	88.62	0.479	
84	19.48	0.96	0.00	66.67	2.09	0.30	89.50	0.624	
85	15.75	0.63	0.05	68.41	1.72	0.35	86.91	0.515	
86	17.41	1.90	0.54	71.82	2.27	0.33	94.27	0.537	
87	47.22	0.20	0.00	47.79	2.44	0.30	97.95		0.883
88	47.27	0.81	0.22	44.02	4.18	0.33	96.83		0.882
				433C-22-5, 45–52 cm					
89	23.43	1.28	0.16	67.75	2.25	0.57	95.44	0.712	
90	21.09	0.86	0.00	71.20	1.11	0.67	94.93	0.631	
91	29.47	0.73	0.00	62.00	1.84	0.48	94.52	0.898	
92	25.27	0.71	0.00	68.48	1.70	0.55	96.71	0.747	
93	21.44	1.06	0.03	71.63	1.34	0.50	96.00	0.636	
94	20.11	0.94	0.00	72.68	1.44	0.46	95.63	0.598	
95	50.52	0.20	0.00	46.13	2.34	0.47	99.66		0.938
96	50.07	0.20	0.15	45.61	2.85	0.47	99.35		0.928
97	50.63	0.24	0.00	45.69	2.90	0.43	99.89		0.933
98	50.60	0.43	0.11	46.61	2.43	0.47	100.65		0.932
99	29.50	1.46	1.97	64.45	2.75	0.50	100.63	0.875	
				433C-24-7, 133–139 cm					
100	19.99	1.82	0.00	66.74	1.41	0.34	90.30	0.637	
101	24.57	1.50	0.00	62.95	1.73	0.35	91.10	0.779	
102	51.19	0.19	0.00	42.61	3.19	0.37	97.55		0.968
103	52.05	0.24	0.00	41.95	3.43	0.29	97.96		0.981
104	49.46	0.29	0.00	44.00	3.20	0.38	97.33		0.932
105	52.17	0.27	0.00	41.14	3.46	0.30	97.34		0.991
106	50.72	0.26	0.00	43.87	2.71	0.27	97.83		0.960
107	51.14	0.29	0.00	41.98	5.51	0.34	99.26		0.921
108	50.78	0.28	0.00	45.16	3.03	0.34	99.59		0.938
109	53.18	0.19	0.00	39.43	3.88	0.42	97.10		1.013
				433C-28-2, 73–80 cm					
110	17.39	1.92	0.00	74.25	0.93	0.37	94.86	0.522	
111	21.13	1.68	0.00	70.35	1.15	0.42	94.73	0.638	
112	23.72	1.72	0.00	69.11	1.27	0.46	96.28	0.708	
113	24.75	1.56	0.00	68.27	1.32	0.59	96.49	0.738	
114	25.33	1.70	0.00	68.09	1.26	0.50	96.88	0.752	
115	25.05	1.67	0.00	68.48	1.36	0.49	97.05	0.743	
116	28.74	1.49	0.03	61.60	1.33	0.64	93.83	0.887	
117	48.84	0.57	0.00	47.30	1.82	0.38	98.91		0.920
118	47.77	0.25	0.00	48.54	1.14	0.39	98.09		0.910
119	49.67	0.30	0.00	48.39	1.41	0.43	100.20		0.926
120	49.59	0.22	0.00	46.98	1.43	0.36	98.58		0.940
121	48.48	0.34	0.00	47.24	1.48	0.37	97.91		0.924
122	48.52	0.26	0.00	47.45	1.79	0.39	98.41		0.915
				433C-29-1, 112–123 cm					
123	51.70	0.23	0.00	43.30	0.60	0.23	96.06		1.021
124	49.00	0.16	0.00	48.52	0.87	0.41	98.96		0.929
125	48.51	0.24	0.00	48.43	0.73	0.77	98.68		0.923
126	48.57	0.26	0.01	48.88	1.04	0.50	99.26		0.916
127	49.50	0.22	0.00	48.08	0.84	0.36	99.00		0.940
128	48.03	0.24	0.02	49.32	1.03	0.32	98.96		0.908
				433C-29-2, 94–100 cm					
129	22.68	0.94	0.04	68.33	0.87	0.45	93.31	0.690	
130	19.53	1.65	0.00	69.04	0.85	0.34	91.41	0.608	
131	23.97	0.87	0.00	65.05	0.97	0.25	91.11	0.747	
132	25.51	1.00	0.00	66.28	0.90	0.32	94.01	0.771	
133	26.25	1.37	0.00	64.91	1.20	0.46	94.19	0.800	
134	48.05	0.21	0.00	47.08	1.78	0.57	97.69		0.912
135	50.99	0.23	0.00	45.87	1.47	0.36	98.92		0.966
				433C-31-1, 28–34 cm					
136	22.13	1.27	0.07	71.45	1.71	0.42	97.05	0.654	
137	21.61	1.35	0.02	71.74	1.76	0.48	96.96	0.639	
138	18.08	2.18	0.20	73.35	1.51	0.44	95.76	0.544	
139	48.54	0.25	0.00	45.76	2.34	0.46	97.35		0.920
140	49.45	0.45	0.00	45.77	2.36	0.44	98.47		0.930
141	49.18	0.21	0.00	46.43	2.39	0.43	98.64		0.920
142	49.45	0.22	0.00	45.54	2.75	0.39	98.35		0.925
143	49.31	0.21	0.00	46.96	2.81	0.46	99.75		0.906
144	48.77	0.24	0.00	46.50	2.69	0.51	98.71		0.906
145	49.84	0.24	0.00	46.62	2.85	0.52	100.07		0.914
				433C-34-2, 103–111 cm					
146	19.95	1.63	0.06	66.41	0.75	0.37	89.17	0.638	
147	48.40	0.18	0.00	42.33	1.57	0.38	92.86		0.976
148	48.14	0.18	0.00	44.06	1.39	0.39	94.16		0.957
149	51.03	0.11	0.00	40.86	1.52	0.35	93.87		1.023

TABLE 6 – *Continued*

No.	TiO_2	Al_2O_3	Cr_2O_3	FeO	MgO	MnO	Total	Titano-magnetite:x	Hemo-ilmenite:y
				433C-34-7, 114–121 cm					
150	15.30	1.66	0.15	71.31	1.17	2.50	92.09	0.485	
151	11.62	1.96	0.24	77.34	0.86	0.62	92.64	0.357	
152	19.41	2.11	3.28	66.36	2.55	0.43	94.14	0.625	
153	8.42	2.25	0.21	80.93	1.98	0.77	94.56	0.257	
154	44.70	0.30	0.00	46.66	2.93	0.30	94.89		0.853
155	46.52	0.16	0.00	42.90	3.20	0.39	93.17		0.909
156	39.01	0.20	0.00	50.38	3.76	0.44	93.79		0.713
				433C-37-3, 79–87 cm					
157	23.98	1.95	0.00	65.96	0.75	1.86	94.50	0.739	
158	22.76	1.96	0.00	67.54	0.82	0.83	93.91	0.698	
159	23.00	1.88	0.00	69.76	0.53	0.41	95.58	0.686	
160	23.14	1.87	0.00	66.45	0.54	1.82	93.82	0.715	
161	23.70	2.19	0.00	65.49	0.57	1.93	93.88	0.737	
162	24.98	1.77	0.00	67.32	0.92	0.38	95.37	0.751	
163	48.76	0.20	0.00	48.11	1.23	0.37	98.67		0.924
164	48.68	0.22	0.00	48.41	0.88	0.46	98.65		0.926
165	48.30	0.28	0.00	48.41	0.93	0.46	98.38		0.921
166	48.88	0.21	0.00	48.56	1.07	0.44	99.16		0.923
				433C-38-1, 67–76 cm					
167	52.32	0.12	0.00	42.16	3.80	0.41	98.81		0.972
168	49.95	0.16	0.00	45.80	3.25	0.38	99.54		0.916
169	49.87	0.17	0.00	45.17	3.17	0.34	98.72		0.925
170	50.14	0.19	0.00	43.25	3.54	0.39	97.51		0.940
171	48.29	0.20	0.00	46.32	3.17	0.30	98.28		0.894
172	48.08	0.17	0.00	45.95	3.08	0.42	97.70		0.896
173	47.49	0.15	0.00	47.06	2.55	0.43	97.68		0.890
174	47.12	0.21	0.00	46.28	2.57	0.41	96.59		0.894
175	46.52	0.17	0.00	46.04	2.61	0.43	95.77		0.888
176	47.42	0.20	0.00	45.88	2.50	0.38	96.38		0.903
177	46.93	0.13	0.00	45.27	2.49	0.33	95.15		0.905
178	48.21	0.20	0.00	45.54	2.72	0.37	97.04		0.911
179	34.89	1.66	6.47	47.98	4.43	0.39	95.82		0.650
				433C-39-5, 87–94 cm					
180	50.11	0.20	0.04	46.71	2.64	0.28	99.98		0.924
181	50.61	0.21	0.12	46.62	2.51	0.39	100.46		0.931
182	51.71	0.18	0.00	44.93	2.12	0.26	99.20		0.972
183	49.03	0.24	0.02	47.07	2.22	0.36	98.94		0.916
184	49.90	0.21	0.40	44.69	3.00	0.41	98.61		0.933
				433C-40-2, 88–96 cm					
185	48.74	0.24	0.33	46.89	2.98	0.34	99.52		0.898
186	48.49	0.23	0.25	46.67	3.00	0.28	98.92		0.897
187	44.39	0.21	0.46	48.73	3.46	0.32	97.57		0.814
188	41.98	0.22	0.19	50.83	3.55	0.45	97.22		0.757
189	0.45	0.06	0.17	88.71	0.14	0.07	89.60	0.014	
190	0.63	0.07	0.14	88.21	0.25	0.05	89.35	0.019	
				433C-42-1, 56–63 cm					
191	14.10	1.48	0.11	77.71	0.27	0.23	93.90	0.421	
192	17.61	1.98	0.09	75.21	0.26	0.32	95.47	0.522	
193	21.89	1.39	0.03	70.57	0.34	0.33	94.55	0.654	
194	4.88	0.63	0.19	87.26	0.19	0.09	93.24	0.144	
195	12.70	2.45	0.11	79.49	0.29	0.26	95.30	0.377	
196	49.51	0.18	0.13	48.96	0.80	0.45	100.03		0.931
197	49.68	0.20	0.10	46.42	1.74	0.37	98.51		0.940
198	48.45	0.21	0.56	48.55	0.92	0.40	99.09		0.922
199	50.93	0.25	0.20	45.70	0.86	0.36	98.30		0.980
200	48.23	0.20	0.50	48.14	1.27	0.42	98.76		0.916
				433C-42-3, 11–20 cm					
201	25.00	1.67	0.00	65.39	0.34	0.40	92.80	0.768	
202	25.11	1.82	0.00	65.26	0.34	0.35	92.88	0.771	
203	23.64	2.01	0.00	65.53	0.39	0.37	91.94	0.735	
204	24.58	1.84	0.00	65.39	0.35	0.38	92.54	0.758	
205	24.80	1.56	0.00	66.43	0.35	1.66	94.80	0.754	
206	23.91	1.64	0.00	67.21	0.37	1.20	94.33	0.727	
207	23.87	1.80	0.00	65.99	0.19	2.25	94.10	0.736	
208	23.95	1.77	0.00	66.27	0.27	1.61	93.87	0.736	
209	48.65	0.26	0.00	49.01	0.42	0.41	98.75		0.930
210	48.40	0.24	0.00	48.66	0.45	0.43	98.18		0.930
211	51.06	0.16	0.00	45.47	0.59	0.48	97.76		0.988
212	52.01	0.13	0.00	44.72	0.53	0.44	97.83		1.007
				433C-42-5, 85–92 cm					
213	49.38	0.23	0.00	48.86	0.71	0.36	99.54		0.934
214	49.73	0.28	0.00	47.79	0.66	0.28	98.74		0.950
215	49.72	0.25	0.04	49.41	0.73	0.41	100.56		0.931
216	50.66	0.15	0.03	47.59	0.87	0.41	99.71		0.956
217	48.64	0.18	0.39	50.12	1.01	0.39	100.73		0.906
218	49.06	0.20	0.12	48.93	0.58	0.37	99.26		0.932
219	49.42	0.19	0.00	47.51	1.10	0.32	98.54		0.940
220	49.30	0.24	0.04	49.12	0.89	0.30	99.89		0.927
221	18.42	2.12	0.03	73.51	0.52	0.28	94.88	0.552	
222	23.77	1.84	0.00	65.50	0.61	1.25	92.97	0.738	
223	18.24	0.88	0.00	73.90	0.30	0.16	93.48	0.545	
224	25.79	1.59	0.00	63.32	0.53	0.30	91.53	0.804	
225	22.29	1.95	0.00	68.29	0.73	0.35	93.61	0.681	
226	21.20	2.00	0.00	69.61	0.71	0.39	93.91	0.645	

TABLE 6 – *Continued*

No.	TiO_2	Al_2O_3	Cr_2O_3	FeO	MgO	MnO	Total	Titano-magnetite:*x*	Hemo-ilmenite:*y*
				433C-47-5, 92–100 cm					
227	10.41	3.13	0.00	72.91	3.17	0.54	90.16	0.341	
228	10.93	3.10	0.00	73.80	3.40	0.56	91.79	0.353	
229	18.21	0.66	0.00	66.70	5.30	0.37	91.24	0.591	
230	17.85	0.78	0.00	66.88	5.40	0.40	91.31	0.581	
231	17.80	1.83	0.00	67.41	5.07	0.53	92.64	0.576	
232	16.98	1.39	0.00	68.65	5.05	0.50	92.57	0.546	
233	18.25	2.36	0.00	67.20	3.52	0.55	91.88	0.589	
234	17.54	2.46	0.00	67.60	3.36	0.61	91.57	0.568	
				433C-49-2, 17–24 cm					
235	25.96	1.57	0.06	64.41	0.80	0.42	93.22	0.798	
236	23.53	1.40	0.00	65.55	0.87	0.48	91.83	0.732	
237	24.38	1.50	0.34	67.65	0.53	0.39	94.79	0.734	
238	24.48	1.43	0.06	68.15	0.66	0.48	95.26	0.732	
239	23.23	2.30	2.40	67.59	0.50	0.54	96.56	0.708	
240	22.71	1.48	0.74	68.93	0.67	0.52	95.05	0.686	
241	25.92	1.48	0.11	64.71	0.77	0.49	93.48	0.794	
242	26.05	1.62	0.05	64.40	0.88	0.44	93.44	0.800	
243	25.33	1.47	0.05	65.61	1.20	0.48	94.14	0.773	
244	23.83	1.64	1.76	65.96	1.03	0.49	94.71	0.736	
245	25.36	1.44	0.00	65.87	0.93	0.44	94.04	0.772	
246	52.56	0.34	0.00	42.21	2.48	0.29	97.88		1.004
247	52.89	0.33	0.00	41.93	2.49	0.34	97.98		1.010
248	51.76	0.34	0.00	42.71	2.66	0.35	97.82		0.985
249	50.01	0.14	0.00	46.25	0.95	0.55	97.90		0.960
250	49.55	0.19	0.00	46.83	0.79	0.48	97.84		0.953
251	49.54	0.19	0.00	45.42	0.70	0.39	96.24		0.972
252	49.53	0.19	0.00	48.84	0.87	0.56	99.99		0.930
253	49.41	0.18	0.00	48.83	0.89	0.60	99.91		0.928
254	49.87	0.19	0.00	46.72	0.96	0.45	98.19		0.955
255	50.70	0.16	0.00	46.15	0.89	0.43	98.33		0.971

Because of this limitation in resolution, application of the Buddington–Lindsley method requires special caution when subsolidus reactions occurred at the micrometer level.

CONCLUSIONS

Fe-Ti oxides in Leg 55 basalts were analyzed by optical microscope, scanning electron microscope, and X-ray microanalyzer. Substantial differences exist between the states of ferromagnetic minerals in the present samples and in typical oceanic basalts. Leg 55 basalts are characterized by universal occurrence of high-temperature oxidation, a high magnetic stability in consequence of the small effective grain size, and a wide range of composition of the titanomagnetite phase. These are typical properties of subaerial basalts. From these observations, we conclude that Leg 55 basalts (and perhaps most of the Emperor Seamounts basalts) were subaerially erupted, and that subsidence into the sea of the volcanic islands at later dates did not appreciably change the original ferromagnetic minerals. We do not support the widespread opinion that titanomagnetites in basalts of any origin alter to titanomaghemite at ambient temperatures if the basalts are submerged under the sea for a sufficiently long period of time ($\sim 10^7$ years, e.g., Ozima et al., 1974). Leg 55 basalts also contain some titanomaghemites. The degree of low-temperature oxidation in Leg 55 basalts is usually quite low. Low-temperature oxidation is confined to samples where high-temperature oxidation was of low or low to moderate degree, but none of the H and M-H samples contain titanomaghemite. Low-temperature oxidation is abundant in Hole 432A (Ningoku) and absent in Hole 430A (Ōjin). In Hole 433C (Suiko), the occurrence of low-temperature oxidation is not related to either type of rock or depth below the sea floor.

Observations by SEM reveal lamellar structure at a fraction of a micrometer. When ilmenite (and other) lamellae are well developed, the host becomes almost pure magnetite. The existence of spinel lamellae at fine scale was found by X-ray energy-dispersive spectrum. The subdivision of magnetite host by lamellae is undoubtedly related to the nearly single-domain-like stability of

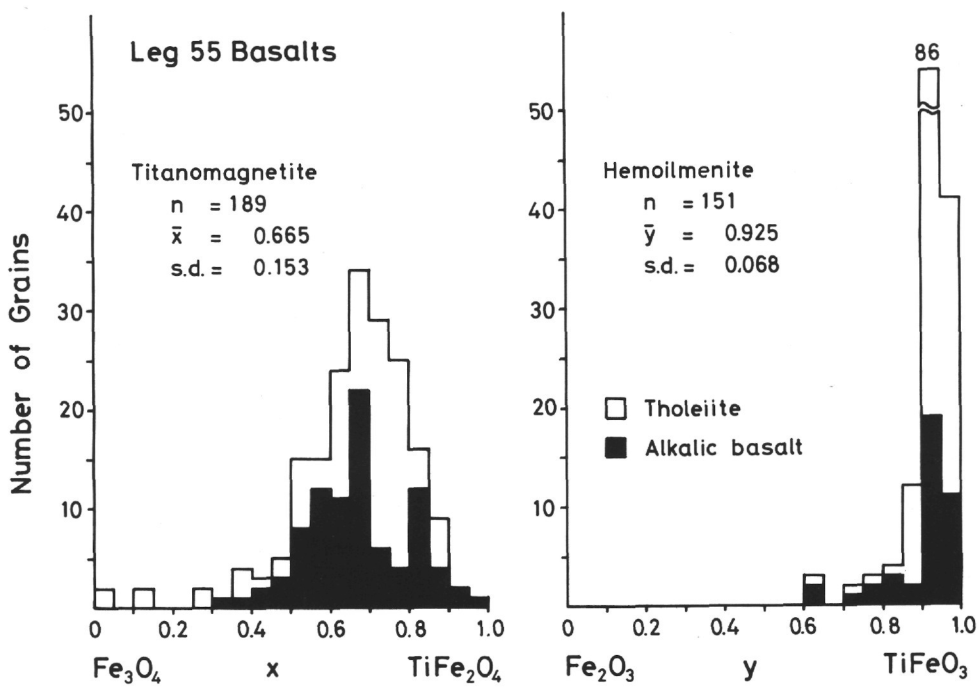

Figure 6. *Distributions of composition parameters* x *of titanomagnetite and* y *of hemoilmenite in Leg 55 basalts, determined by microprobe analyses.*

TABLE 7
Average Compositions of Opaque Minerals

Sample (Interval in cm)	Titanomagnetite n	Titanomagnetite x	Titanomagnetite s.d.	Hemoilmenite n	Hemoilmenite y	Hemoilmenite s.d.	Buddington–Lindsley Temperature (°C)	fO_2 ($-\log fO_2$)
430A-4-2, 110–118	5	0.754	0.181	4	0.866	0.140	1200	8.2
5-1, 21–27	1	0.445		10	0.910	0.099		
5-2, 102–115	5	0.520	0.025	4	0.903	0.005	960	11.4
6-1, 17–25	5	0.584	0.085	4	0.918	0.012	970	11.4
6-3, 52–63	5	0.659	0.058	5	0.980	0.050	790	16.4
6-4, 7–15	5	0.593	0.064	2	0.976	0.081		
6-4, 140–150	4	0.685	0.074	2	0.926	0.001		
432A-2-1, 86–92	7	0.851	0.048					
2-3, 37–43	3	0.850	0.020	2	0.628	0.018		
3-2, 120–126	5	0.681	0.005					
5-2, 57–66	7	0.819	0.012					
433A-20-1, 30–36	5	0.656	0.048					
21-4, 129–138	6	0.563	0.121	2	0.962	0.114		
433B-5-2, 61–68	5	0.680	0.079	2	0.936	0.008		
5-3, 85–90	5	0.676	0.045					
433C-4-1, 30–38	8	0.685	0.022	3	0.920	0.001		
10-4, 11–17	5	0.600	0.205					
12-3, 57–65	5	0.516	0.246					
13-2, 55–66	5	0.773	0.026	5	0.939	0.006	1095	9.9
14-3, 8–15	5	0.808	0.086	5	0.977	0.044	1030	11.5
15-6, 16–31	6	0.744	0.060	2	0.991	0.049		
19-5, 57–65	3	0.701	0.037	5	0.949	0.014		
21-4, 7–13	4	0.539	0.062	2	0.883	0.001		
22-5, 45–52	7	0.728	0.120	4	0.933	0.004	1055	10.5
24-7, 133–139	2	0.708	0.101	8	0.963	0.032	965	12.0
28-2, 73–80	7	0.712	0.112	6	0.923	0.010	1060	10.3
29-1, 112–123				6	0.940	0.041		
29-2, 94–100	5	0.723	0.076	2	0.939	0.038		
31-1, 28–34	3	0.612	0.059	7	0.917	0.009		
34-2, 103–111	1	0.638		3	0.985	0.034		
34-7, 114–121	4	0.431	0.160	3	0.825	0.101		
37-3, 79–87	6	0.721	0.025	4	0.923	0.002	1055	10.4
38-1, 67–76				13	0.891	0.076		
39-5, 87–94				5	0.935	0.022		
40-2, 88–96	2	0.016	0.004	4	0.841	0.069		
42-1, 56–63	5	0.423	0.189	5	0.938	0.025	820	14.2
42-3, 11–20	8	0.748	0.017	4	0.964	0.040	980	11.8
42-5, 85–92	6	0.661	0.103	8	0.935	0.015	995	11.3
47-5, 92–100	8	0.518	0.107					
49-2, 17–24	11	0.751	0.038	10	0.967	0.028	980	12.0

Notes: fO_2 in atmospheres. All the samples from Hole 433C, except 433C-4-1, 30–38 cm and 433C-47-5, 92–100 cm, are tholeiites. All the samples from the other holes are alkalic basalts (including hawaiites).

magnetization in these rocks. Because of such fine-scale structures in Fe-Ti oxides, we point out the inherent ambiguity in application of the Buddington–Lindsley method to estimate the "last" equilibrium temperatures and oxygen fugacities.

ACKNOWLEDGMENTS

We are indebted to Penny Patterson (University of Colorado) for help in preparation of samples for and operation of the SEM. Yozo Hamano and Tadashi Nishitani (University of Tokyo) gave valuable comments. The Department of Microbiology of the University of Colorado kindly permitted us to use their SEM. The expenses of M.K. while in Boulder were defrayed by DSDP. We would like to express our gratitude to these persons and institutions.

REFERENCES

Ade-Hall, J. M., Khan, M. A., Dagley, P., and Wilson, R. L., 1968. A detailed opaque petrological and magnetic investigation of a single Tertiary lava flow from Skye, Scotland—I. Iron-titanium oxide petrology, *Geophys. J. Roy. Astron. Soc.,* v. 16, pp. 375–388.

Ade-Hall, J. M., Palmer, H. C., and Hubbard, T. P., 1971. The magnetic and opaque petrological response of basalts to regional hydrothermal alteration, *Geophys. J. Roy. Astron. Soc.,* v. 24, pp. 137–174.

Akimoto, S. and Kushiro, I., 1960. Natural occurrence of titanomaghemite and its relevance to the unstable magnetization of rocks, *J. Geomag. Geoelect.,* v. 11, pp. 94–110.

Buddington, A. F. and Lindsley, D. H., 1964. Iron-titanium oxide minerals and synthetic equivalents, *J. Petrol.,* v. 5, pp. 310–357.

Carmichael, I. S. E. and Nicholls, J., 1967. Iron-titanium oxides and oxygen fugacities in volcanic rocks, *J. Geophys. Res.,* v. 72, pp. 4665–4687.

Creer, K. M. and Ibbetson, J. D., 1970. Electron microprobe analysis and magnetic properties of non-stoichiometric titanomagnetites in basaltic rocks, *Geophys. J. Roy. Astron. Soc.,* v. 21, pp. 485–511.

Hamano, Y., Nishitani, T., and Kono, M., in press. Magnetic properties of basalt samples from Holes 417D and 418A. *In* Donnelly, T., Francheteau, J., Bryan, W., Robinson, P., Flower, M., Salisbury, M., et al., *Initial Reports of the Deep Sea Drilling Project,* v. 51, 52, 53, Part 2: Washington (U.S. Government Printing Office).

Johnson, H. P. and Atwater, T., 1977. Magnetic study of basalts from the Mid-Atlantic Ridge, lat. 37°N, *Geol. Soc. Am. Bull.,* v. 88, pp. 637–647.

Johnson, H. P. and Hall, J. M., 1978. A detailed rock magnetic and opaque mineralogy study of the basalts from the Nazca Plate, *Geophys. J. Roy. Astron. Soc.,* v. 52, pp. 45–64.

Katsura, T., Kitayama, K., and Aoyagi, R., 1976. High temperature experiments concerning the Fe–Ti oxide minerals, *Kazan (J. Volcanol. Soc. Japan),* v. 21, pp. 31–56 (in Japanese with English abstract).

Larson, E. E., Ozima, M., Ozima, M., Nagata, T. and Strangway, D., 1969. Stability of remanent magnetization of igneous rocks, *Geophys. J. Roy. Astron. Soc.,* v. 17, pp. 263–292.

Lowrie, W., 1977. Intensity and direction of magnetization in oceanic basalts, *J. Geol. Soc.,* v. 133, pp. 61–82.

Marshall, M., 1978. The magnetic properties of some DSDP basalts from the north Pacific and inferences for Pacific plate tectonics, *J. Geophys. Res.,* v. 83, pp. 289–308.

Ozima, M. and Larson, E. E., 1970. Low- and high-temperature oxidation of titanomagnetite in relation to irreversible changes in the magnetic properties of submarine basalts, *J. Geophys. Res.,* v. 75, pp. 1003–1017.

Ozima, M., Joshima, M., and Kinoshita, H., 1974. Magnetic properties of submarine basalts and the implications on the structure of the oceanic crust, *J. Geomag. Geoelectr.,* v. 26, pp. 335–354.

Petersen, N., 1976. Notes on the variation of magnetization within basalt lava flows and dykes, *Pure Appl. Geophys.,* v. 114, pp. 177–193.

Readman, P. W. and O'Reilly, W., 1972. Magnetic properties of oxidized (cation-deficient) titanomagnetites (Fe, Ti, □)$_3$O$_4$, *J. Geomag. Geoelectr.,* v. 24, pp. 69–90.

Strangway, D. W., Larson, E. E., and Goldstein, M., 1968. A possible cause of high magnetic stability in volcanic rocks, *J. Geophys. Res.,* v. 73, pp. 3789–3795.

Wilson, R. L. and Haggarty, S. E., 1966. Reversals of the earth's magnetic field, *Endeavour,* v. 25, pp. 104–109.